Enhanced purinergic signaling in the paraventricular hypothalamus induces hyperphagic obesity and insulin resistance

Yu Liu[1], Haiyang Zhang[2], Qian Zhang[3], Syeda Sadia Najam[1], Xian Liang[4], Chaweewan Sirakawin[1], Dongfa Lin[1,5], Shangyuan Huang[1], Anastasiia Bondarenko[1], Witold Konopka[6], Yi Zhang[7], Zhi Zhang[8], Shihao Wu[3,*], Miao Jing[2,*], Ilya A. Vinnikov[1,*]

[1] Laboratory of Molecular Neurobiology, Sheng Yushou Center of Cell Biology and Immunology, Department of Genetics and Developmental Biology, School of Life Sciences and Biotechnology, Shanghai Jiao Tong University, Shanghai, China.

[2] Chinese Institute for Brain Research, Beijing, China.

[3] School of Medicine, Yunnan University, Kunming, Yunnan, China.

[4] Human Phenome Institute, Fudan University, Shanghai, China.

[5] Key Laboratory for Molecular Enzymology and Engineering, School of Life Sciences, Jilin University; Changchun, China.

[6] Laboratory of Neuroplasticity and Metabolism, Department of Life Sciences and Biotechnology, Łukasiewicz PORT Polish Center for Technology Development, Wrocław, Poland.

[7] Shanghai Diabetes Institute, Shanghai Key Laboratory of Diabetes Mellitus, Shanghai Clinical Centre for Diabetes, Shanghai Sixth People's Hospital Affiliated to Shanghai Jiao Tong University School of Medicine, Shanghai, China.

[8] School of Life Sciences, Fudan University, Shanghai, China.

*Corresponding authors: IAV, ilya.vinnikov@gmail.com; MJ, jingmiao@cibr.ac.cn; SW, brad-315@163.com.

Abstract

Body energy homeostasis is tightly regulated by hypothalamic neural circuits. However, their remodeling upon metabolic stress remains incompletely characterized, translating to unprecedented challenges to develop safe medications against the surge of metabolic diseases. Oxytocin (OXT) neurons in the paraventricular nucleus of the hypothalamus (PVH) are one of the key appetite-suppressing effectors within the melanocortin system. In this work, we report that metabolic stress in mice evokes spatiotemporally selective ATP release (Inflares) from PVH astrocytes, accompanied with the expression of hematopoietic lineage-specific ADP/ATP receptor $P2Y_{12}$ on OXT (PVH^{OXT}) neurons. Importantly, "ectopic" emergence of $P2Y_{12}$ on OXT neurons of patients with diabetes mellitus suggests an evolutionary conserved purinergic response to metabolic stress. Strikingly, increased purinergic signaling leads to impaired responsiveness of PVH^{OXT} neurons accompanied with hyperphagic obesity and insulin resistance in mice. Moreover, nasal administration of clinically approved doses of $P2Y_{12}$ inhibitors counteracts diet-induced obesity and insulin resistance in mice and spontaneous weight gain in monkeys, paving the way for their application in patients with metabolic disorders.

Running title: Nasal application of $P2Y_{12}$ inhibitors reverses obesity and normalizes insulin sensitivity.

More than one billion people suffer from obesity [1], which contributes to associated metabolic disorders, such as diabetes mellitus. Pharmacological approaches to treat these conditions include inhibitors of pancreatic lipases, agonists of receptors for glucagon-like peptide-1 and for glucose-dependent insulinotropic polypeptide [2]. However, the requirement of long-term application of these compounds for weight maintenance is associated with potential side effects [3], underscoring a pressing need for identifying novel targets and more effective drug delivery strategies [4]. Centrally acting pharmaceuticals represent a promising alternative, but are required to effectively cross the blood-brain barrier (BBB) when delivered systemically [5]. With the advantage of the unique anatomical and physiological connection between the nasal cavity and the brain [6], nasal delivery of pharmaceuticals emerges as a potential solution to both bypass the BBB and mitigate peripheral side effects [7-9].

Within the brain, the key neuronal circuits regulating energy homeostasis, such as the melanocortin system, are located in the hypothalamus [10,11]. Melanocortinergic projections from the first order neurons release α-melanocyte stimulating hormone (α-MSH) in the paraventricular nucleus of the hypothalamus (PVH) to induce satiety [12-14] via activation of $G\alpha_s$-coupled melanocortin 4 receptor (MC4R) on the second order neurons [15,16] . Subsequently, MC4R activation initiates the adenylyl cyclase/cAMP/phosphorylation cascade leading to the expression of Fos proto-oncogene, activator protein 1 (AP-1) transcription factor subunit (or c-Fos), which is critical for neuronal activity of these second order cells [17-25]. A metabolically critical subset of these MC4R-positive second order neurons in PVH releases oxytocin (OXT) to suppress appetite [26-29]. Metabolic disorders have been found to be associated with the dysfunction in purinergic system [30], which is composed of versatile extracellular ligands and membrane receptors mediating cell-cell communication to regulate immune, hemostasis, endocrine and other functions [31-33]. Recently, we identified a stress-evoked spatiotemporally selective pattern of ATP release from astrocytes, named Inflares, representing an active signal transmission system that encodes brain injury properties [34]. The matching between injury and Inflares ensures the adequate damage management, emphasizing the importance of purinergic signaling as well as its alteration that might contribute to disease progression. Such purinergic signal transmission system might also exist in the hypothalamus, reacting on metabolic challenges and encoding stress information to affect the activity of ATP-sensing cells. At the receiver side, a major ATP/ADP receptor $P2Y_{12}$, encoded by the *P2ry12* gene, was found to be exclusively expressed on microglia [35,36]. Yet a direct binding and activation of the *P2ry12* gene promoter by its upstream transcriptional regulator NF-κB is known to be stimulated by metabolic stress [37], which also activates this transcription factor in microglia [38,39] and hypothalamic neurons [40,41]. It is unclear whether hypothalamic neurons with activated NF-κB signaling could turn on the "ectopic" expression of $P2Y_{12}$, thus being able to act as another decoder of the extracellular purinergic signals.

Given the tight link between purinergic signaling and metabolic diseases [30,33], while keeping in mind the need of identifying novel therapeutic strategies for their treatment, we aimed here to delineate the pathophysiological mechanisms, metabolic function, and relevance of this pathway within the hypothalamus.

Results

Metabolic stress induces ATP release within PVH

First, we tested whether, in analogy with other types of brain injuries [34], metabolic stress, such as western diet or diabetes, may induce ATP Inflares within PVH, the critical region regulating energy intake and expenditure. We stereotaxically injected recombinant adeno-associated viral vector (rAAV) encoding the ATP1.0 sensor into PVH of adult mice fed with high-fat diet (HFD) or normal chow food. Next, using two-photon microscopy, we recorded

the extracellular ATP dynamics in acute PVH slices from these mice. Remarkably, starting from as early as two weeks of HFD feeding, we observed a gradual increase in the frequency of Inflares in PVH compared to unchanged levels in chow diet-fed animals (**Fig. 1a,b, Movies S1-S2**). Notably, unaltered amplitude, size and duration of individual Inflares between time points of HFD feeding are consistent with our recent report that individual Inflares serve as the fundamental signaling unit (**Fig. S1a-c**). Furthermore, pre-treatment with probenecid, the inhibitor of the pannexin 1 channel, reduced the Inflares in HFD-treated mice (**Fig. 1c,d, Movie S3**), supporting the hemichannel-dependent mechanism of ATP release [34]. To explore whether other types of metabolic stress can up-regulate purinergic signaling, we analyzed the ATP dynamics in PVH of mice with streptozotocin-induced type I diabetes mellitus. Consistent with the HFD model, we observed an elevated frequency of Inflares in diabetic mice (**Fig. 1e,f, Movie S4**), supporting that metabolic stress induces selective patterns of astrocytic ATP release that contributes to altered purinergic signaling within PVH.

Metabolic stress induces an "ectopic" expression of $P2Y_{12}$ on PVH^{OXT} neurons

Next, we sought to investigate how these Inflares signal within PVH of metabolically compromised mice. Strongly enriched in this region [42] (**Fig. S1d**) and reported to be exclusively expressed in microglia within the central nervous system [36,43], $P2Y_{12}$ is a G_i-protein coupled receptor that could sense ATP/ADP in Inflares. Surprisingly, HFD induced an "ectopic" expression of this microglia-specific receptor on 54.67 ± 3.62% PVH^{OXT} neurons (**Fig. 1g**) vs. no expression in PVH^{OXT} neurons of chow-fed animals ($p < 0.0001$). To validate these results, we analyzed the levels of *P2ry12* in FACS-isolated PVH^{OXT} neurons from HFD-fed mice prior to the onset of obesity (**Fig. S1e**) and detected a drastic up-regulation of this transcript compared to animals fed with chow diet (**Fig. 2h**). Next, we examined whether similar "ectopic" emergence of $P2Y_{12}$ on OXT neurons can also be induced by other types of metabolic stressors, for example in human patients with diabetes mellitus. Strikingly, we also detected a strong OXT neuron-specific expression of human $P2Y_{12}$ receptor in post-mortem tissues from three out of four investigated patients with diabetes mellitus (**Fig. 1i, Table S1**). In agreement with previous studies [40,41], we detected altered expression patterns of NF-κB-associated transcripts in PVH^{OXT} neurons of obese and diabetic cynomolgus monkeys (*Macaca fascicularis*) [44], suggesting a potential role of this pathway in upregulating its direct downstream target [37] $P2Y_{12}$ (**Fig. S1f**). Altogether, we describe here that neuronal expression of $P2Y_{12}$ accompanied with elevation of ATP Inflares constitutes a novel purinergic pathway in the metabolically stressed hypothalamus.

Inhibition of $P2Y_{12}$ reverses obesity in mice

Next, we hypothesized that $G\alpha_i$-dependent inactivation of the adenylyl cyclase/cAMP/cFos axis downstream of $P2Y_{12}$ antagonizes the MC4R/$G\alpha_s$ signaling in the second order melanocortin system cells (**Fig. 2a**). Indeed, over-expression of $P2Y_{12}$ in hypothalamic GT1-7 cells reduced intracellular cAMP levels, leading to a diminished expression of *Fos* and inability of α-MSH to elicit transcriptional response in these cells (**Fig. 2b-e**). With the objective to explore *in vivo* the contribution of elevated $P2Y_{12}$ signaling in metabolic regulation and obesity phenotype, we orally administered HFD-fed mice with 90 mg/kg/day dose [45] of ticlopidine, a prodrug of an irreversible inhibitor of $P2Y_{12}$ which is capable to cross BBB. Indeed, such a huge dose (27 times the human daily recommended dose) of ticlopidine rapidly reversed the diet-induced obesity, suggesting that ATP signaling contributes to the progression of this metabolic phenotype (**Fig. S2a, Table 1**). Notably, we failed to rescue the obesity phenotype in HFD mice by high doses (27 times the human daily recommended dose) of other irreversible $P2Y_{12}$ inhibitor prodrugs, such as clopidogrel and

prasugrel, or by lower concentrations (9 times the human daily recommended dose) of ticlopidine, which revealed only a tendency towards weight decrease, not reaching a statistical significance (**Fig. S2b**).

Nasal administration of $P2Y_{12}$ inhibitors reverses diet-induced obesity

To lower the administered doses of $P2Y_{12}$ inhibitors to the levels that are recommended in humans for daily peroral administration, while maintaining high concentrations in the brain, we conceptualized a nasal way of delivery (**Fig. 3a**). Rewardingly, nasal administration of irreversible inhibitor prodrugs ticlopidine, prasugrel, but not vehicle or clopidogrel, in clinically relevant peroral human doses once a day, rapidly reversed obesity and attenuated fat mass accumulation in HFD-fed mice (**Fig. 3b-d, Table 1**). Notably, the anti-obesity effect of ticlopidine was lost upon further halving of the dose (**Fig. S2c**), indicating that the human daily recommended peroral dose might approach to the minimal effective concentration in mice. Both ticlopidine and prasugrel normalized HFD-induced adipocyte hypertrophy, fasting glucose levels and the performance in the insulin tolerance test (**Fig. 3e-g, Table 1**). Interestingly prasugrel, but not ticlopidine, managed to fully restore insulin sensitivity, judging by the glucose tolerance test (**Fig. 3h, Table 1**). Mechanistically the anti-obesity effects of the $P2Y_{12}$ inhibitors are mostly attributed to the reduction in food intake (**Fig. 3i**), with minor effect in the restoration of energy expenditure (**Fig. S3**).

To identify the lowest effective dose, we halved the human daily recommended doses for prasugrel, as well as for the two reversible $P2Y_{12}$ inhibitors cangrelor and ticagrelor (**Fig. 4a**). Interestingly, similar to irreversible inhibitor prodrugs, both cangrelor and ticagrelor demonstrated a strong anti-obesity potential at clinically relevant doses when administered nasally (**Fig. 4b-c, S4a, Table 1**), with cangrelor being the only $P2Y_{12}$ inhibitor demonstrating effectiveness in mice at subhuman concentrations. These results suggest that the human daily recommended peroral doses might approach to the minimal effective concentrations of other three inhibitors in mice. Importantly, we used nucleic magnetic resonance spectroscopy to verify the abundance of a nasally administered ticagrelor and its metabolites in the hypothalamus (**Fig. S4b**). Interestingly, even after withdrawal of the nasal administration of ticagrelor or cangrelor, the animals did not start regaining weight (**Fig. 4d**). While both cangrelor and ticagrelor normalized food intake, fasting glucose levels and performance at insulin tolerance test, only cangrelor managed to fully restore the insulin sensitivity, as indicated by glucose tolerance test (**Fig. 4e-g, Table 1**). Indeed, ticagrelor significantly attenuated, but failed to normalize the performance in the latter assay.

Finally, we sought to use $P2Y_{12}$ blockers to reverse obesity in *M. fascicularis*. In agreement with previous reports [46], about 15% of aged *M. fascicularis* in our facility tend to voraciously consume all *ad libitum* provided food, developing obesity. Hence, such animals are subjected to calorie-restricted conditions to prevent age-associated pathologies [47-49]. In our experimental design, we lifted the chow diet restriction in such animals by 80% while simultaneously administering once-a-day nasal spray with human daily recommended doses of cangrelor or vehicle (**Fig. 4h**). In agreement with our results in mice, cangrelor protected macaques from weight gain not only during the nasal administration, but also eight weeks after withdrawal of the drug (**Fig. 4i-k**). These data further support an evolutionary conserved role of purinergic signaling in metabolic control and provide a translational perspective for nasal administration of $P2Y_{12}$ inhibitors to treat metabolic diseases.

Over-expression of $P2Y_{12}$ in PVH^{OXT} neurons drives obesity in mice

To explore the sufficiency of the ectopic $P2Y_{12}$ expression to induce obesity, we next over-expressed this receptor specifically in PVH^{OXT} neurons of adult mice by transducing $OXT^{IRES\text{-}Cre}$ mice with AAV-CMV-FLEX-P2ry12-GFP vector (**Fig. 5a, S5a,b**). Indeed, these PVH^{OXT}:$P2Y_{12}$ mice fed with normal chow diet developed obesity, which could be reversed

by nasally administered prasugrel in human daily recommended dose (**Fig. 5b,c**), with no regain of weight even after withdrawal of the drug (**Fig. 5d**). Consistently, the $P2Y_{12}$-overexpressing OXT neurons in the PVH became less responsive to hyperosmotic stress (**Fig. 5e,f**) which is known to stimulate OXT neurons [50]. Notably, when fed with chow diet, PVH^{OXT}:$P2Y_{12}$ mice also developed insulin resistance and hyperphagia, which could be reversed by nasal prasugrel administration (**Fig. 5g-i**). In agreement with our previous data, a tendency towards a decreased energy expenditure in $P2Y_{12}$-overeexpressing mice did not reach a statistical significance (**Fig. S6**), suggesting that the weight gain-promoting effect of the over-activated purinergic signaling is mainly driven by hyperphagia. Accordingly, reversal of obesity by $P2Y_{12}$ inhibitors largely, if not completely, relies on their anorexigenic action, in agreement with studies demonstrating appetite-suppressing effects of OXT [26,51,52]. Altogether, hyperphagic obesity and insulin resistance induced by "ectopic" $P2Y_{12}$ expression on PVH^{OXT} neurons can be reversed by the inhibitors of this ADP/ATP receptor, confirming its causative obesogenic role.

Discussion

Understanding the metabolic stress-induced signaling changes in the hypothalamic circuits is key to develop effective therapeutic strategies. Our results indicate that the metabolic stress stimulates and profoundly reorganizes purinergic signaling in PVH by linking OXT neurons into the pathological signaling loop. Increased appetite and insulin resistance caused by the "ectopic" expression of $P2Y_{12}$ on PVH^{OXT} neurons can be attenuated by the nasal administration of human recommended daily doses of inhibitors of this ATP/ADP receptor.

The gradual time-dependent elevation of ATP release in PVH of HFD-exposed mice suggests that individual Inflares encode the extent of the metabolic damage. Interestingly, in diabetic, but not HFD-treated mice, elevated frequency of Inflares was accompanied by increased duration of the ATP release, suggesting different modalities of purinergic signals encoding a specific type of metabolic stress. Previously we reported that the information encoded by Inflares can be efficiently retrieved and further transduced by microglia as the key decoder [34], which may lead to inflammation-associated reactive microgliosis [16,53], also detected by us in the PVH from patients with diabetes mellitus.

Here we identified that in addition to microglia, OXT neurons within both supraoptic nucleus (unpublished data) and PVH may be context-dependently converted to yet another decoder, resulting in aggravation of pathological phenotypes associated with the metabolic stress. Importantly, the "ectopic" HFD-induced $P2Y_{12}$ expression on OXT neurons emerges prior to the onset of weight gain. Interestingly, this evolutionary conserved context-dependent "ectopic" expression may be related to the duration or extent of diabetes. Indeed, out of the four examined brains from patients suffering from this condition, two revealed 19.2% and 81.1% PVH^{OXT} neurons strongly positive for $P2Y_{12}$ and one more patient revealed no PVH^{OXT}, but about half of supraoptic nucleus OXT neurons strongly positive for $P2Y_{12}$ (unpublished data). The latter observation suggests that various populations of OXT (and possibly other) neurons might react to metabolic stress or other injuries with different timing and/or dynamics, leading to alterations of the purinergic signaling and reshaping the neuronal circuits. Overall, apart from the pathological role in exacerbation of the metabolic phenotypes, the epigenetic landscape of these cell populations might be permissive also for stress-related contexts or other not yet explored conditions to promote the occurrence of $P2Y_{12}$-dependent physiological modalities of OXT neurons.

Our *in vitro* data about attenuation of the responsiveness of hypothalamic neurons by $P2Y_{12}$ overexpression was validated by the gain-of-function Cre-LoxP-FLEX model. Indeed, c-Fos expression was markedly down-regulated in PVH^{OXT} neurons of PVH^{OXT}:$P2Y_{12}$ mice. In addition, we demonstrated an obesogenic sufficiency of the "ectopic" $P2Y_{12}$ overexpression on PVH^{OXT} neurons, since both hyperphagic obesity and insulin resistance could be induced

even without high calorie diets. Further support of the causative or at least contributing obesogenic role of $P2Y_{12}$ comes from the loss-of-function model (LY, SH, DL, SSN, WK, IAV, manuscript in preparation) demonstrating that knock-out of $P2Y_{12}$ specifically in PVH^{OXT} neurons can attenuate obesity. Yet another confirmation of the causation or contribution of $P2Y_{12}$ comes from the rapid and highly reproducible effect of multiple inhibitors of this ATP/ADP receptor.

Indeed, peroral administration of ticlopidine in high doses reverses obesity, while nasal administration of prasugrel, ticlopidine, ticagrelor and cangrelor in clinically relevant doses normalizes food intake, weight and insulin sensitivity. The latter inhibitor was also effective in a form of nasal spray to prevent age-associated weight gain in non-human primates, opening the possibility to explore the application of $P2Y_{12}$ inhibitors in humans. Indeed, since OXT neurons of patients suffering from diabetes mellitus start expressing this ATP/ADP receptor, which per se is capable to drive hyperphagic obesity and insulin resistance, pharmacological inhibition of $P2Y_{12}$ might relieve these metabolic symptoms. Nevertheless, we may not rule out that anti-obesity effects of $P2Y_{12}$ inhibitors rely at least in part on microglia, which may also respond to metabolic stress-induced Inflares and indirectly alter anorexigenic circuits within the hypothalamus. Delineating the selective or synergistic effects of purinergic signaling connecting multiple cell types in the hypothalamus is worth further exploration.

Notably, when delivered in extremely high concentrations exceeding the human daily dose by 40 times, clopidogrel, a prodrug of the irreversible $P2Y_{12}$ inhibitor, was reported to significantly reduce body weight and recovery rates in the stroke mouse model, while a phase IV FDA-approved clinical study demonstrated unintentional weight loss in 3528 patients (2.5%) receiving this inhibitor [54]. Our experiments demonstrated that perorally administered 27 times the daily recommended human dose of another prodrug ticlopidine, but not clopidogrel, was able to counteract obesity. Consistently, the metabolic symptoms were effectively reversed by nasal administration of clinically relevant doses of the prodrugs ticlopidine and prasugrel, which were plausibly converted to irreversible $P2Y_{12}$ inhibitors by the brain-derived cytochrome P450. Although expressed at much lower levels than in the liver, this enzyme is abundant in the frontal cortex and the hypothalamus, particularly in astrocytes [55-57]. The successful biodistribution of nasally administered $P2Y_{12}$ inhibitors within the brain opens a perspective for this way of delivery of these pharmaceuticals for alleviation the metabolic symptoms.

Notably, nasal administration of $P2Y_{12}$ inhibitors reversed obesity, but resulted in no further weight reduction beyond the normal weight either in chow or HFD-fed animals, while also not gaining weight even after withdrawal of the drugs. These results suggest that the observed anti-obesity effect is not merely a consequence of appetite blockade, but rather remodels dysfunctional hypothalamic circuits that contribute to the excessive weight gain. Another interesting observation relates to the differential effect on insulin sensitivity restoration by different $P2Y_{12}$ inhibitors, suggesting that it is not merely a consequence of weight alleviation. Indeed, despite both ticlopidine and ticagrelor fully restored the performance of mice in the insulin tolerance test, these inhibitors, failed to normalize the performance in the glucose tolerance test. In contrast, prasugrel and cangrelor, successfully restored the insulin tolerance test performance, with ticagrelor being partially, but significantly effective to attenuate it. These results suggest that the alleviation of insulin sensitivity by $P2Y_{12}$ inhibitors is uncoupled or not completely dependent on their anti-obesity function, in agreement with the direct effects of OXT neurons in preventing insulin resistance, independent from anorexigenic function [51,58].

In conclusion, we have demonstrated that metabolic stress induces ATP Inflares and pathological "ectopic" expression of $P2Y_{12}$ on PVH^{OXT} neurons, while nasal administration of $P2Y_{12}$ blockers can rapidly reverse diet-induced obesity, paving the way for these widely used pharmaceuticals as potent therapeutics to combat metabolic diseases.

Materials and Methods

Animal models

All experimental procedures in mice of both genders were conducted on the C57BL/6 genetic background (at least nine backcrosses) at Shanghai Jiao Tong University and Chinese Institute for Brain Research in accordance with international standards, as approved by the institutional and local authorities of China. B6;129S-Oxt$^{tm1.1(cre)Dolsn}$/J, referred to as OXT$^{IRES-Cre}$, mice [59] and a tdTomato reporter line B6.Cg-Gt(ROSA)26Sor$^{tm14(CAG-tdTomato)Hze}$/J [60] (Jackson laboratory, 024234 and 007914, respectively) were crossed visualize OXT neurons. Tissue digestion protocol before fluorescence-activated cell sorting (FACS) was followed as described elsewhere [61] (see also **Extended Materials and Methods** for more details).

Experiments on cynomolgus macaques (*Macaca fascicularis*) were conducted in accordance with the guidelines of the National Institute of Health's Guide for the Care and Use of Laboratory Animals and approved by the Ethics Committee of Kunming Medical University. A cohort of six obese male macaques aged between 8 to 16 years with body weights ranging from 8.7 to 10.85 kg was individually housed in cages with dimensions of 0.74 m x 0.71 m x 0.74 m, under standard environmental conditions, at 25 ± 2°C, a 14-hour light/10-hour dark cycle, and a relative humidity of 60% with ad libitum access to water (for further details, please refer to **Table S2** and **Extended Materials and Methods**).

In vivo administration of compounds

For peroral administration with drinking water and/or nasal delivery, ticlopidine, clopidogrel, prasugrel hydrochloride, ticagrelor (all from APExBIO; B2164, A5183, B1283, B2166, respectively) and cangrelor tetrasodium (MedChemExpress, 163706-36-3) were used at concentrations indicated in the figures. For the control groups, normal drinking water was used in experiments with peroral administration, 0.9% NaCl for experiments shown in **Fig. 3, 5** and **S2c**, **S3**, **S4**, 10% DMSO (Sigma-Aldrich, D2650) in 0.9% NaCl for experiments shown in **Fig. 4**. For nasal delivery in mice according to [9], 1-2 µl at a time were alternately and slowly delivered to the entrance of each nostril (total volume of 20 µl was applied within 3-5 min) to aid the uptake from the nasal sinus through the sifter plate into the olfactory bulb and spread to the mouse brain. 700 MHz nuclear magnetic resonance (NMR) AVANCE NEO spectrometer (Bruker) was used to analyze the abundance of ticagrelor within the hypothalamus at the Instrumental Analysis Center of Shanghai Jiao Tong University. A spray in a total volume of 50 µl once per day was administered nasally to cynomolgus monkeys.

For salt loading experiments, 90 minutes after hyperosmotic stimulation of OXT neurons by intraperitoneal injection of 15 ml/kg 1.5 M NaCl [62] the isolated brain were fixed in 4% paraformaldehyde (PFA) for subsequent analyses.

Cell Culture

The mouse hypothalamic GT1-7 and human kidney HEK293T cell lines were purchased from the Cell Bank of Shanghai Institutes for Biological Sciences, China and cultured in DMEM (Gibco, 11960044) containing 10% fetal bovine serum (Hyclone, SV30087.03), 100 U/ml penicillin and 100 U/ml streptomycin at 37°C and 5% CO_2. The growth of cells was observed daily, with the culture medium replaced daily or every other day according to the conditions of the cells.

For *in vitro* $P2Y_{12}$ overexpression, mouse *P2ry12* cDNA was subcloned into pCDH-EF1-copGFP-T2A-Puro (Addgene, 72263, a gift from Kazuhiro Oka) at EcoRI and BamHI sites. The resulting Lenti-P2ry$_{12}$OE construct was packaged, transduced in GT1-7 cells and 72 hours later FACS-sorted into 6-well plates, followed by verification of clones by qRT-PCR. GT1-7

cells were treated by α-MSH (100 nM) for 15 mins to induce cAMP and downstream targets [63].

Statistical analysis

Statistical analysis was performed in GraphPad Prism software (version 9.0) using Shapiro-Wilk normality test, Kruskal-Wallis test followed by Dunn's multiple comparisons test, Wilcoxon rank-sum test, two-tailed paired or unpaired Student's t-tests, one- or two-way ANOVA followed by Holm-Šídák's post-hoc tests against all groups, unless otherwise stated (see figure legends for details). Group numbers indicate biological replicates. Results are presented as means ± standard errors of means (SEM). *p*-values of less than 0.05 were considered statistically significant: *, $p < 0.05$; **, $p < 0.01$; ***, $p<0.001$; ****, $p<0.0001$.

Acknowledgments

The authors gratefully acknowledge Haixia Jiang for help with cell sorting, Bo Wang for technical assistance, Jieli Wu for NMR analysis, Ali Alamdar and Tatyana Grinenko for assistance with image analysis, Ruslan Konovalov for computational analyses. We very much thank Hui Lu, Juliang Chen and Honglei Xiao for sectioning of and Anna Berliand for anatomic insights in human brain tissues, Tiemin Liu for invaluable discussions and assistance with obtaining expression data from patients and non-human primates, Vladimir Popov for the technical details of nasal administration, Cheng Hu and Valery Grinevich for the support, Nicola Murgia for the help with animal management. DNA visualization in **Fig. 2a** is from vecteezy.com. This work was funded by the Special project of the Ministry of Life Sciences and the Ministry of Medical Sciences C0800399 and Research Fund for International Scientists BC0800441 from the National Natural Science Foundation of China (NSFC) to IAV; 32371150 from NSFC, the National Key Research and Development Program 2021YFE0116400, the STI2030-Major project 2021ZD0202200, Subject 2021ZD0202203 to MJ; 82101241 and 82360226 grants from NSFC to SW.

Author contributions

Conceptualization: IAV

Methodology: YL, HZ, SW, MJ, IAV

Investigation: YL, HZ, QZ, SSN, XL, DL, YZ, SH, AB, CS, WK, MJ, IAV

Visualization: YL, HZ, DL, IAV

Funding acquisition: SW, MJ, IAV

Project administration: IAV

Supervision: SW, MJ, IAV

Writing – original draft: YL, MJ, IAV

Writing – review & editing: YL, MJ, IAV

All authors reviewed and contributed to the manuscript.

Competing interests: YL and IAV have filed related patents. The remaining authors declare no competing interests.

Data and materials availability: All data are available in the main text or the supplementary materials.

References

1 Worldwide trends in underweight and obesity from 1990 to 2022: a pooled analysis of 3663 population-representative studies with 222 million children, adolescents, and adults. *Lancet* **403**, 1027-1050, doi:10.1016/s0140-6736(23)02750-2 (2024).

2 Chakhtoura, M. *et al.* Pharmacotherapy of obesity: an update on the available medications and drugs under investigation. *eClinicalMedicine* **58**, doi:10.1016/j.eclinm.2023.101882 (2023).

3 Lenharo, M. Anti-obesity drugs' side effects: what we know so far. *Nature* **622**, 682, doi:10.1038/d41586-023-03183-3 (2023).

4 Blüher, M. *et al.* New insights into the treatment of obesity. *Diabetes, obesity & metabolism* **25**, 2058-2072, doi:10.1111/dom.15077 (2023).

5 Keller, L. A., Merkel, O. & Popp, A. Intranasal drug delivery: opportunities and toxicologic challenges during drug development. *Drug delivery and translational research* **12**, 735-757, doi:10.1007/s13346-020-00891-5 (2022).

6 Patel, D. & Thakkar, H. Formulation considerations for improving intranasal delivery of CNS acting therapeutics. *Therapeutic delivery* **13**, 371-381, doi:10.4155/tde-2022-0018 (2022).

7 Jeong, S. H., Jang, J. H. & Lee, Y. B. Drug delivery to the brain via the nasal route of administration: exploration of key targets and major consideration factors. *Journal of pharmaceutical investigation* **53**, 119-152, doi:10.1007/s40005-022-00589-5 (2023).

8 Hanson, L. R. & Frey, W. H., 2nd. Intranasal delivery bypasses the blood-brain barrier to target therapeutic agents to the central nervous system and treat neurodegenerative disease. *BMC neuroscience* **9 Suppl 3**, S5, doi:10.1186/1471-2202-9-s3-s5 (2008).

9 Gómez-Pinedo, U. *et al.* Intranasal Administration of Undifferentiated Oligodendrocyte Lineage Cells as a Potential Approach to Deliver Oligodendrocyte Precursor Cells into Brain. *International journal of molecular sciences* **22**, doi:10.3390/ijms221910738 (2021).

10 Waterson, M. J. & Horvath, T. L. Neuronal Regulation of Energy Homeostasis: Beyond the Hypothalamus and Feeding. *Cell metabolism* **22**, 962-970, doi:10.1016/j.cmet.2015.09.026 (2015).

11 Tran, L. T. *et al.* Hypothalamic control of energy expenditure and thermogenesis. *Experimental & molecular medicine* **54**, 358-369, doi:10.1038/s12276-022-00741-z (2022).

12 Millington, G. W. The role of proopiomelanocortin (POMC) neurones in feeding behaviour. *Nutrition & metabolism* **4**, 18, doi:10.1186/1743-7075-4-18 (2007).

13 Xu, Y. *et al.* Glutamate mediates the function of melanocortin receptor 4 on Sim1 neurons in body weight regulation. *Cell metabolism* **18**, 860-870, doi:10.1016/j.cmet.2013.11.003 (2013).

14 Sohn, J. W. Network of hypothalamic neurons that control appetite. *BMB reports* **48**, 229-233, doi:10.5483/bmbrep.2015.48.4.272 (2015).

15 Krashes, M. J., Lowell, B. B. & Garfield, A. S. Melanocortin-4 receptor-regulated energy homeostasis. *Nature neuroscience* **19**, 206-219, doi:10.1038/nn.4202 (2016).

16 Zhang, W., Xiao, D., Mao, Q. & Xia, H. Role of neuroinflammation in neurodegeneration development. *Signal transduction and targeted therapy* **8**, 267, doi:10.1038/s41392-023-01486-5 (2023).

17 Granell, S., Mohammad, S., Ramanagoudr-Bhojappa, R. & Baldini, G. Obesity-linked variants of melanocortin-4 receptor are misfolded in the endoplasmic reticulum and can be rescued to the cell surface by a chemical chaperone. *Molecular endocrinology (Baltimore, Md.)* **24**, 1805-1821, doi:10.1210/me.2010-0071 (2010).

18 Ramírez, D. *et al.* Melanocortin 4 receptor activates ERK-cFos pathway to increase brain-derived neurotrophic factor expression in rat astrocytes and hypothalamus. *Molecular and cellular endocrinology* **411**, 28-37, doi:10.1016/j.mce.2015.04.008 (2015).
19 Yang, L. K. & Tao, Y. X. Biased signaling at neural melanocortin receptors in regulation of energy homeostasis. *Biochimica et biophysica acta. Molecular basis of disease* **1863**, 2486-2495, doi:10.1016/j.bbadis.2017.04.010 (2017).
20 Chai, B. *et al.* Melanocortin-4 receptor-mediated inhibition of apoptosis in immortalized hypothalamic neurons via mitogen-activated protein kinase. *Peptides* **27**, 2846-2857, doi:10.1016/j.peptides.2006.05.005 (2006).
21 Sutton, G. M., Duos, B., Patterson, L. M. & Berthoud, H. R. Melanocortinergic modulation of cholecystokinin-induced suppression of feeding through extracellular signal-regulated kinase signaling in rat solitary nucleus. *Endocrinology* **146**, 3739-3747, doi:10.1210/en.2005-0562 (2005).
22 Patten, C. S., Daniels, D., Suzuki, A., Fluharty, S. J. & Yee, D. K. Structural and signaling requirements of the human melanocortin 4 receptor for MAP kinase activation. *Regulatory peptides* **142**, 111-122, doi:10.1016/j.regpep.2007.02.005 (2007).
23 He, S. & Tao, Y. X. Defect in MAPK signaling as a cause for monogenic obesity caused by inactivating mutations in the melanocortin-4 receptor gene. *International journal of biological sciences* **10**, 1128-1137, doi:10.7150/ijbs.10359 (2014).
24 Wang, Y. & Prywes, R. Activation of the c-fos enhancer by the erk MAP kinase pathway through two sequence elements: the c-fos AP-1 and p62TCF sites. *Oncogene* **19**, 1379-1385, doi:10.1038/sj.onc.1203443 (2000).
25 Glas, E., Mückter, H., Gudermann, T. & Breit, A. Exchange factors directly activated by cAMP mediate melanocortin 4 receptor-induced gene expression. *Scientific reports* **6**, 32776, doi:10.1038/srep32776 (2016).
26 Tolson, K. P. *et al.* Postnatal Sim1 deficiency causes hyperphagic obesity and reduced Mc4r and oxytocin expression. *The Journal of neuroscience : the official journal of the Society for Neuroscience* **30**, 3803-3812, doi:10.1523/jneurosci.5444-09.2010 (2010).
27 Blevins, J. E. & Ho, J. M. Role of oxytocin signaling in the regulation of body weight. *Reviews in endocrine & metabolic disorders* **14**, 311-329, doi:10.1007/s11154-013-9260-x (2013).
28 Liu, H. *et al.* Transgenic mice expressing green fluorescent protein under the control of the melanocortin-4 receptor promoter. *J Neurosci* **23**, 7143-7154, doi:10.1523/jneurosci.23-18-07143.2003 (2003).
29 Maejima, Y., Yokota, S., Nishimori, K. & Shimomura, K. The Anorexigenic Neural Pathways of Oxytocin and Their Clinical Implication. *Neuroendocrinology* **107**, 91-104, doi:10.1159/000489263 (2018).
30 de Oliveira, M. *et al.* Pitfalls and challenges of the purinergic signaling cascade in obesity. *Biochemical pharmacology* **182**, 114214, doi:10.1016/j.bcp.2020.114214 (2020).
31 Burnstock, G. Purinergic signalling in endocrine organs. *Purinergic signalling* **10**, 189-231, doi:10.1007/s11302-013-9396-x (2014).
32 Zarrinmayeh, H. & Territo, P. R. Purinergic Receptors of the Central Nervous System: Biology, PET Ligands, and Their Applications. *Molecular imaging* **19**, 1536012120927609, doi:10.1177/1536012120927609 (2020).
33 Huang, Z. *et al.* From purines to purinergic signalling: molecular functions and human diseases. *Signal transduction and targeted therapy* **6**, 162, doi:10.1038/s41392-021-00553-z (2021).

34 Chen, Y. *et al.* Spatiotemporally selective astrocytic ATP dynamics encode injury information sensed by microglia following brain injury in mice. *Nature neuroscience*, doi:10.1038/s41593-024-01680-w (2024).
35 Haynes, S. E. *et al.* The P2Y12 receptor regulates microglial activation by extracellular nucleotides. *Nature neuroscience* **9**, 1512-1519, doi:10.1038/nn1805 (2006).
36 Cserép, C. *et al.* Microglia monitor and protect neuronal function through specialized somatic purinergic junctions. *Science (New York, N.Y.)* **367**, 528-537, doi:10.1126/science.aax6752 (2020).
37 Hu, L. *et al.* Platelets Express Activated P2Y(12) Receptor in Patients With Diabetes Mellitus. *Circulation* **136**, 817-833, doi:10.1161/circulationaha.116.026995 (2017).
38 Valdearcos, M. *et al.* Microglial Inflammatory Signaling Orchestrates the Hypothalamic Immune Response to Dietary Excess and Mediates Obesity Susceptibility. *Cell Metab* **26**, 185-197.e183, doi:10.1016/j.cmet.2017.05.015 (2017).
39 Wang, Z. *et al.* Saturated fatty acids activate microglia via Toll-like receptor 4/NF-κB signalling. *The British journal of nutrition* **107**, 229-241, doi:10.1017/s0007114511002868 (2012).
40 Zhang, X. *et al.* Hypothalamic IKKbeta/NF-kappaB and ER stress link overnutrition to energy imbalance and obesity. *Cell* **135**, 61-73, doi:10.1016/j.cell.2008.07.043 (2008).
41 Shih, R. H., Wang, C. Y. & Yang, C. M. NF-kappaB Signaling Pathways in Neurological Inflammation: A Mini Review. *Front Mol Neurosci* **8**, 77, doi:10.3389/fnmol.2015.00077 (2015).
42 Lein, E. S. *et al.* Genome-wide atlas of gene expression in the adult mouse brain. *Nature* **445**, 168-176, doi:10.1038/nature05453 (2007).
43 Bennett, M. L. *et al.* New tools for studying microglia in the mouse and human CNS. *Proceedings of the National Academy of Sciences of the United States of America* **113**, E1738-1746, doi:10.1073/pnas.1525528113 (2016).
44 Lei, Y. *et al.* Region-specific transcriptomic responses to obesity and diabetes in macaque hypothalamus. *Cell metabolism* **36**, 438-453.e436, doi:10.1016/j.cmet.2024.01.003 (2024).
45 Jawien, J. *et al.* Ticlopidine attenuates progression of atherosclerosis in apolipoprotein E and low density lipoprotein receptor double knockout mice. *European journal of pharmacology* **556**, 129-135, doi:10.1016/j.ejphar.2006.11.028 (2007).
46 Vaughan, K. L. & Mattison, J. A. Obesity and Aging in Humans and Nonhuman Primates: A Mini-Review. *Gerontology* **62**, 611-617, doi:10.1159/000445800 (2016).
47 DeLany, J. P., Hansen, B. C., Bodkin, N. L., Hannah, J. & Bray, G. A. Long-term calorie restriction reduces energy expenditure in aging monkeys. *The journals of gerontology. Series A, Biological sciences and medical sciences* **54**, B5-11; discussion B12-13, doi:10.1093/gerona/54.1.b5 (1999).
48 Cefalu, W. T. *et al.* Caloric restriction and cardiovascular aging in cynomolgus monkeys (Macaca fascicularis): metabolic, physiologic, and atherosclerotic measures from a 4-year intervention trial. *The journals of gerontology. Series A, Biological sciences and medical sciences* **59**, 1007-1014, doi:10.1093/gerona/59.10.b1007 (2004).
49 Colman, R. J. *et al.* Caloric restriction delays disease onset and mortality in rhesus monkeys. *Science (New York, N.Y.)* **325**, 201-204, doi:10.1126/science.1173635 (2009).
50 Wang, S. C., Parpura, V. & Wang, Y. F. Astroglial Regulation of Magnocellular Neuroendocrine Cell Activities in the Supraoptic Nucleus. *Neurochem Res* **46**, 2586-2600, doi:10.1007/s11064-020-03172-2 (2021).
51 Camerino, C. Low sympathetic tone and obese phenotype in oxytocin-deficient mice. *Obesity (Silver Spring, Md.)* **17**, 980-984, doi:10.1038/oby.2009.12 (2009).

52 McCormack, S. E., Blevins, J. E. & Lawson, E. A. Metabolic Effects of Oxytocin. *Endocrine reviews* **41**, 121-145, doi:10.1210/endrev/bnz012 (2020).
53 Di Virgilio, F., Vultaggio-Poma, V., Falzoni, S. & Giuliani, A. L. Extracellular ATP: A powerful inflammatory mediator in the central nervous system. *Neuropharmacology* **224**, 109333, doi:10.1016/j.neuropharm.2022.109333 (2023).
54 Paul, M. *et al.* Clopidogrel Administration Impairs Post-Stroke Learning and Memory Recovery in Mice. *International journal of molecular sciences* **24**, doi:10.3390/ijms241411706 (2023).
55 Mansour, A., Bachelot-Loza, C., Nesseler, N., Gaussem, P. & Gouin-Thibault, I. P2Y(12) Inhibition beyond Thrombosis: Effects on Inflammation. *International journal of molecular sciences* **21**, doi:10.3390/ijms21041391 (2020).
56 Wijeyeratne, Y. D. & Heptinstall, S. Anti-platelet therapy: ADP receptor antagonists. *British journal of clinical pharmacology* **72**, 647-657, doi:10.1111/j.1365-2125.2011.03999.x (2011).
57 Ferguson, C. S. & Tyndale, R. F. Cytochrome P450 enzymes in the brain: emerging evidence of biological significance. *Trends in pharmacological sciences* **32**, 708-714, doi:10.1016/j.tips.2011.08.005 (2011).
58 Papazoglou, I. *et al.* A distinct hypothalamus-to-β cell circuit modulates insulin secretion. *Cell metabolism* **34**, 285-298.e287, doi:10.1016/j.cmet.2021.12.020 (2022).
59 Wu, Z. *et al.* An obligate role of oxytocin neurons in diet induced energy expenditure. *PloS one* **7**, e45167, doi:10.1371/journal.pone.0045167 (2012).
60 Madisen, L. *et al.* A robust and high-throughput Cre reporting and characterization system for the whole mouse brain. *Nature neuroscience* **13**, 133-140, doi:10.1038/nn.2467 (2010).
61 Yu, Y. *et al.* Interneuron origin and molecular diversity in the human fetal brain. *Nature neuroscience* **24**, 1745-1756, doi:10.1038/s41593-021-00940-3 (2021).
62 Giovannelli, L., Shiromani, P. J., Jirikowski, G. F. & Bloom, F. E. Oxytocin neurons in the rat hypothalamus exhibit c-fos immunoreactivity upon osmotic stress. *Brain research* **531**, 299-303, doi:10.1016/0006-8993(90)90789-e (1990).
63 Mohammad, S. *et al.* Constitutive traffic of melanocortin-4 receptor in Neuro2A cells and immortalized hypothalamic neurons. *The Journal of biological chemistry* **282**, 4963-4974, doi:10.1074/jbc.M608283200 (2007).

Supplementary Information

Extended Materials and Methods

Figs. S1 to S6

Tables S1 to S2

Movies S1 to S4

Table 1. Summary of metabolic activities analyzed for $P2Y_{12}$ inhibitors.

$P2Y_{12}$ inhibitor	Way	Dose (mg/kg/d)	Reduction				
			Weight (maximal)†	Food intake‡	GTT AUC‡	ITT AUC‡	Fasting glucose‡
Ticlopidine	Oral	90	27.41 ± 5.30% after 3.4 wk, p = 0.00575	Not analyzed	Not analyzed	Not analyzed	Not analyzed
	Nasal	3.57	38.27 ± 2.39% after 3.1 wk, p = 0.00019	56.89 ± 14.4%, p = 0.00294	8.31 ± 11.0%, p = 0.4615	86.93 ± 22.5%, p = 0.0039	34.03 ± 8.18%, p = 0.0181 6.9 ± 0.3 mmol/L
Prasugrel	Nasal	0.14	28.83 ± 6.1% after 3.1 wk, p = 0.0103	51.05 ± 15.6%, p = 0.00553	37.56 ± 11.4%, p = 0.0118	78.35 ± 23.5%, p = 0.00537	33.65 ± 14.36%, p = 0.0181 6.94 ± 1.26 mmol/L
Ticagrelor	Nasal	2.40	20.73 ± 4.84% after 2.7 wk, p = 0.00793	64.29 ± 13.1%, p = 0.00023	10.4 ± 9.4%, p = 0.2923	54.47 ± 19.6%, p = 0.0172	29.2 ± 9.95%, p = 0.0252 6.54 ± 0.28 mmol/L
Cangrelor	Nasal	0.18	24.49 ± 2.21% after 2.7 wk, p = 0.00018	75.30 ± 13.1%, p < 0.0001	34.7 ± 9.4%, p = 0.00636	61.43 ± 19.6%, p = 0.0172	31.6 ± 12.87%, p = 0.0252 6.32 ± 0.8 mmol/L

† Maximal weight reduction detected in this study, with the differences before vs. after drug administration in mice with diet-induced obesity ± standard error of means (SEM), statistically analyzed by paired two-tailed Student's t-test (from experiments depicted in **Fig. S2a, 3b** and, for cangrelor and ticagrelor, **4b**). Notably, the latter two drugs were first administered with half a human daily dose for periods indicated in **Fig. 4a**.

‡ Reduction of the area under the curve (AUC) of cumulative food intake, glucose (GTT) or insulin tolerance tests (ITT) and 4 hr-fasting blood glucose levels vs. the HFD-Vehicle groups in the experiments depicted in **Fig. 3g-i, 4e-g** ± SEM, statistically analyzed by one-way ANOVA followed by Holm-Šídák's post hoc test. Baseline of 0 g and 4 mmol/l was used for food intake and tolerance tests, respectively. Additionally, absolute 4 hr-fasting glucose levels are depicted.

Figure 1

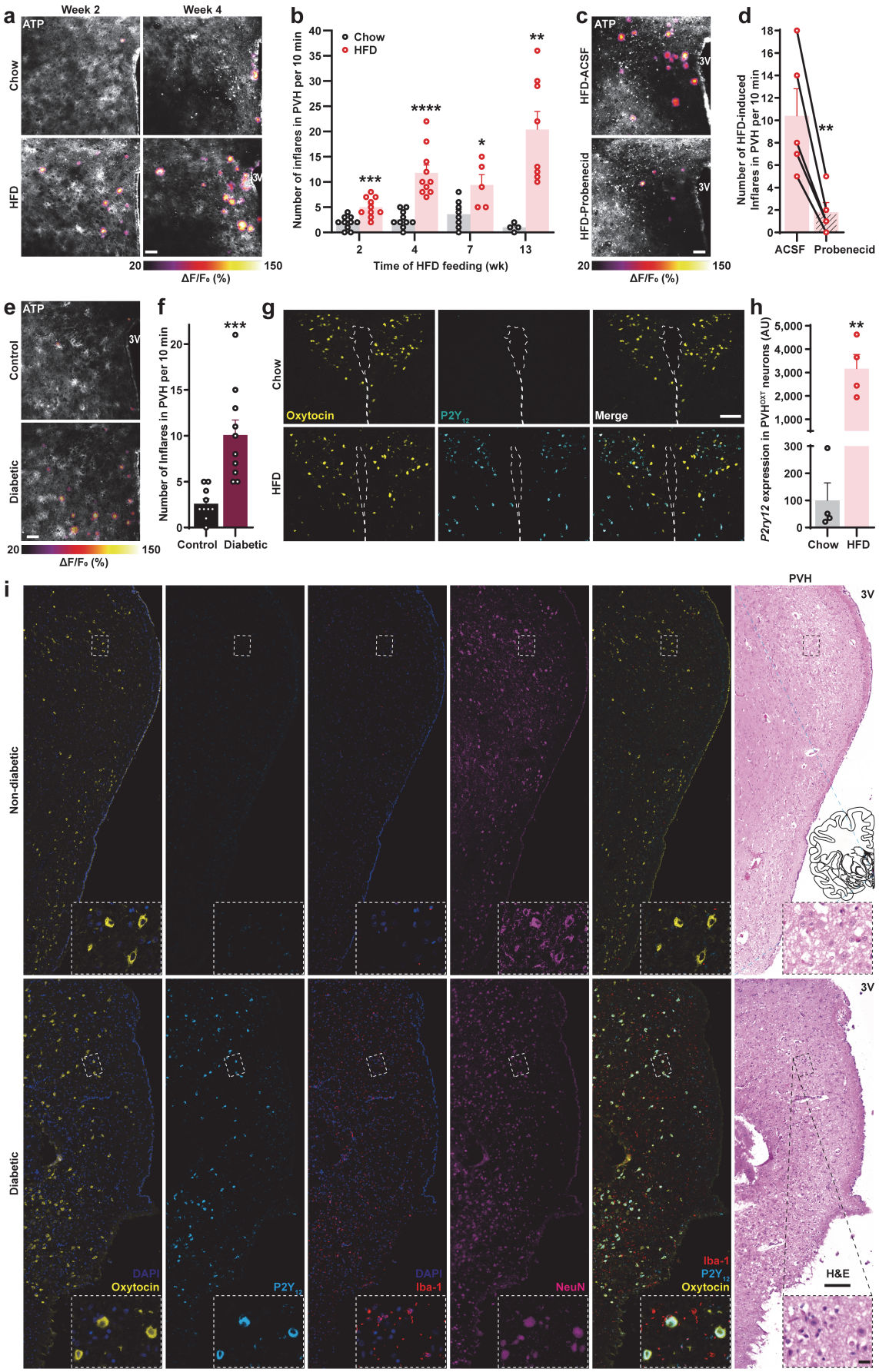
a
Week 2
Week 4
ATP
Chow
HFD
3V
20
150
ΔF/F₀ (%)
b
Chow
HFD
Number of inflares in PVH per 10 min
Time of HFD feeding (wk)
2
4
7
13
***
****
*
**
c
ATP
HFD-ACSF
HFD-Probenecid
3V
20
150
ΔF/F₀ (%)
d
Number of HFD-induced Inflares in PVH per 10 min
ACSF
Probenecid
**
e
ATP
Control
Diabetic
3V
20
150
ΔF/F₀ (%)
f
Number of Inflares in PVH per 10 min
Control
Diabetic
***
g
Chow
HFD
Oxytocin
P2Y12
Merge
h
P2ry12 expression in PVHOXT neurons (AU)
Chow
HFD
**
i
Non-diabetic
Diabetic
PVH
3V
DAPI
Oxytocin
P2Y12
DAPI
Iba-1
NeuN
Iba-1
P2Y12
Oxytocin
H&E

Fig. 1. Metabolic stress induces ATP release and "ectopic" expression of $P2Y_{12}$ on PVH^{OXT} neurons. (**a-b**) Representative microphotographs (**a**) and quantification (**b**) of the ATP Inflares in PVH regions-containing acute hypothalamic slices of male mice fed with chow or high-fat diet (HFD) for indicated time periods (2 and 4 wk analyses: n = 10 from 3 mice per group; 7 wk: n = 8 and 5 from 3 mice; 13 wk: n= 4 and 8 from 3 mice for Chow and HFD groups, respectively). The peak fluorescence change ($\Delta F/F_0$) of Inflares recorded by the ATP1.0 sensor over 10 minutes are pseudocolored for better visualization. The frequency of Inflares over 10 min recording were quantified. (**c-d**) Representative microphotographs (**c**) and quantification (**d**) of Inflares in PVH-containing acute slices of male mice fed with HFD for 4 wk before and after treatment with probenecid (n = 5 slices from 3 mice). (**e-f**) Representative microphotographs (**e**) and quantification (**f**) of Inflares in male mice 2 wk after streptozotocin or vehicle injection (n = 10 slices from 3 mice from each group). (**g**) Representative confocal microphotographs of the hypothalamic slices immunostained for $P2Y_{12}$ from $OXT^{IRES\text{-}Cre}$-driven reporter male mice fed with HFD for 10 wk (n = 4). (**h**) qRT-PCR analysis of *P2ry12* in FACS-isolated PVH^{OXT} neurons of female mice fed with HFD for 4 wk (n = 4). (**i**) Co-localization microphotographs of the PVH-containing *ex vivo* slices from patients with or without diabetes mellitus (n = 4 and 3, respectively). Error bars represent standard error of means (SEM). * $p < 0.05$, ** $p < 0.01$, *** $p < 0.001$, **** $p < 0.0001$ as analyzed by unpaired (**b**,**f**,**h**) or paired (**d**) two-tailed Student's t-tests. Scale bar in µm: 50 (**a**,**c**,**e**), 100 (**g**), 200 (**i**) and 20 (insets in **i**).

Figure 2

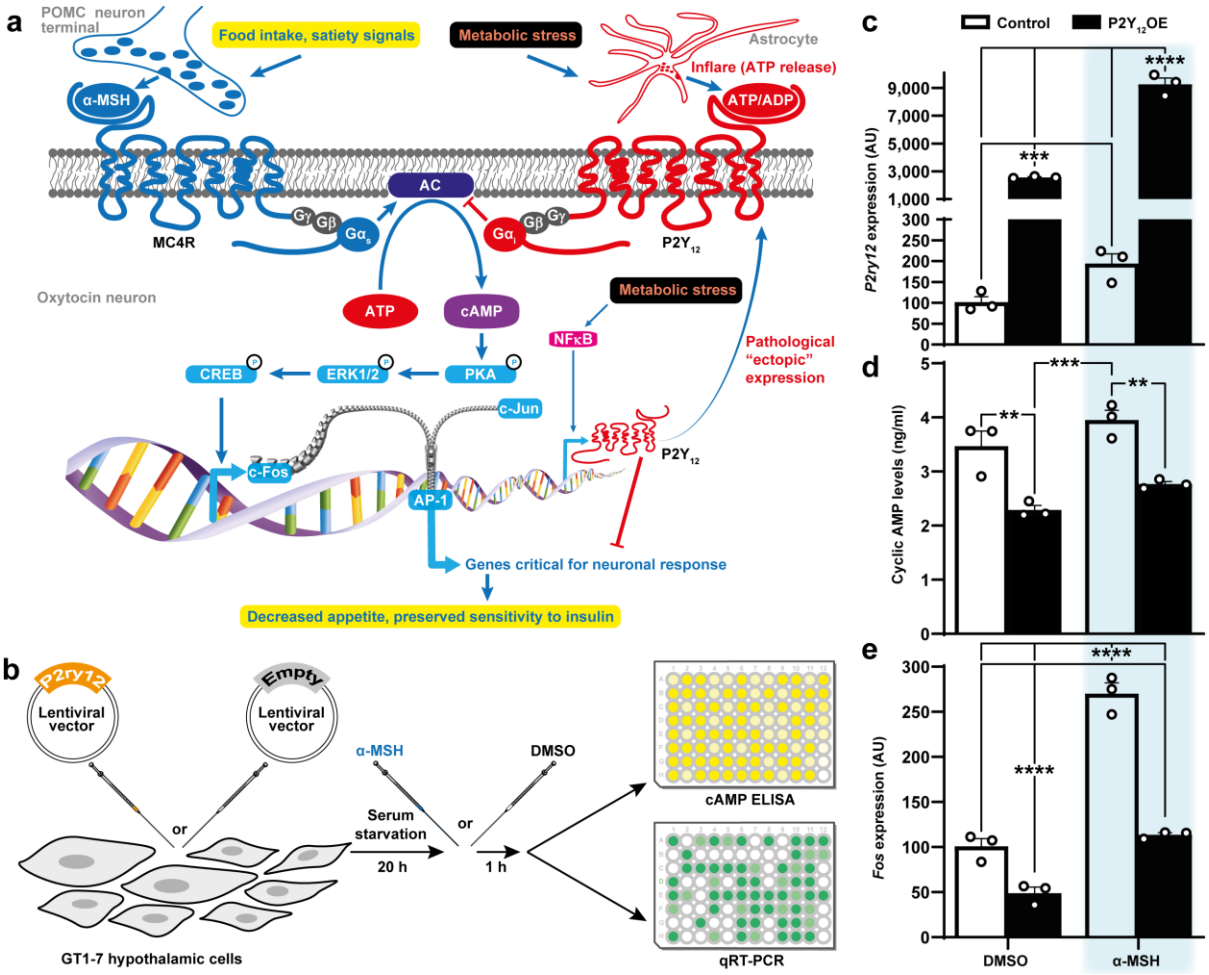

Fig. 2. P2Y$_{12}$ diminishes responsiveness of hypothalamic cells. (**a**) Schematic representation of the hypothetic mechanism involving purinergic pathway interactions within PVH^{OXT} neurons. (**b-e**) GT1-7 hypothalamic cells were transduced with a lentiviral overexpressing *P2ry12* followed by α-MSH-mediated stimulation and analysis. Experimental design (**b**) and analyses by qRT-PCR (**c, e**) or ELISA (**d**) of *P2ry12* (**c**), cAMP (**d**) and *Fos* (**e**) (n = 3). Error bars represent SEM. ** $p < 0.01$, *** $p < 0.001$, **** $p < 0.0001$ as analyzed by one-way ANOVA followed by post-hoc Holm-Šídák's test.

Figure 3

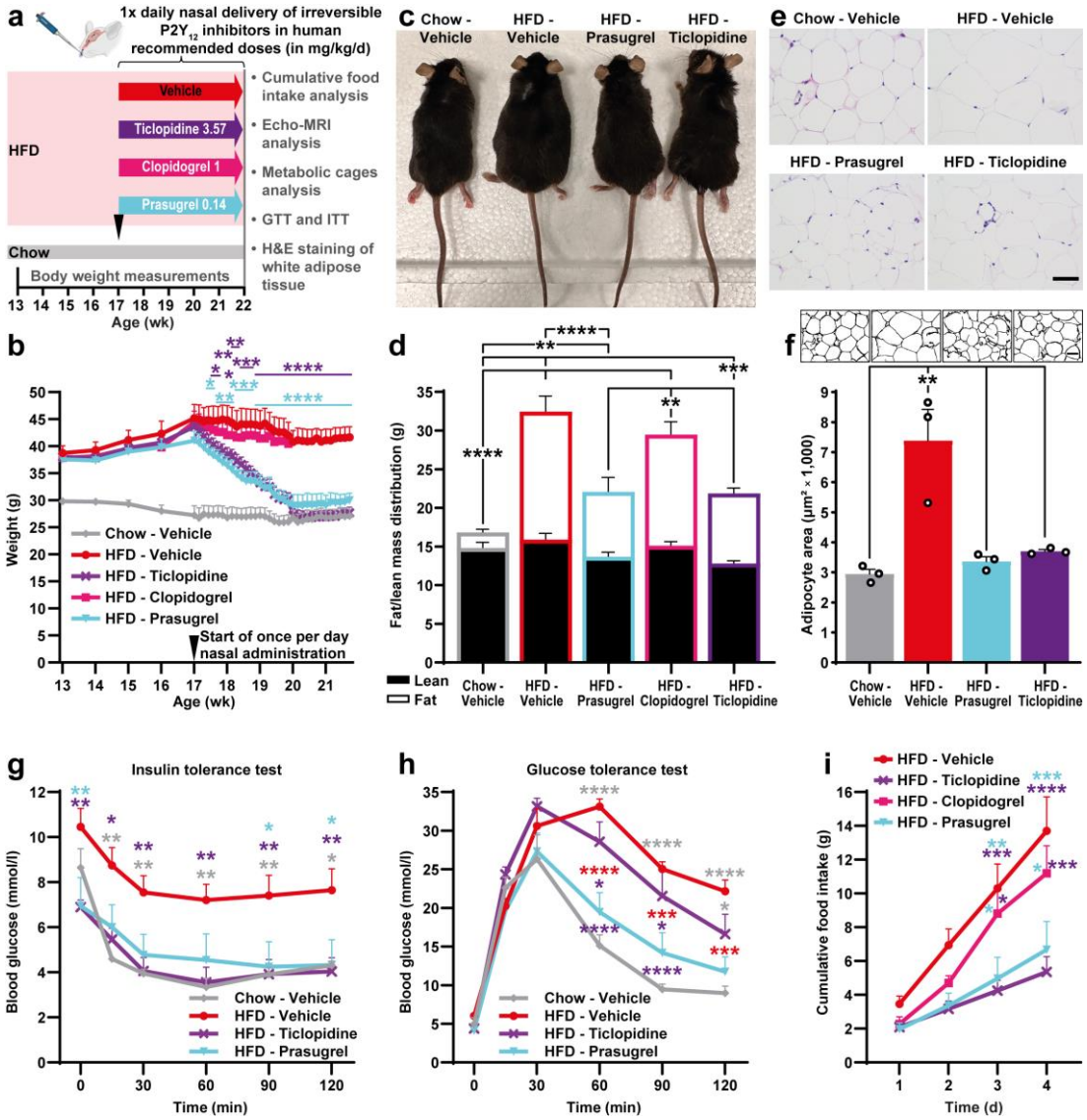

Fig. 3. Nasal administration of $P2Y_{12}$ inhibitors reverses diet-induced obesity and hyperphagia in mice. (**a-i**) Experimental design (**a**), weight (**b**), representative photograph (**c**), Echo-MRI-based fat/lean mass distribution analysis on Week 20 (**d**), representative microphotographs (**e**) with adipocyte edges detection and area quantification of hematoxylin and eosin-stained perigonadal white adipose tissue (**f**, n = 3), insulin (**g**) and glucose (**h**) tolerance tests, cumulative food intake on Week 20 (**i**) in HFD-fed male mice nasally administered once a day with 1 mg/kg clopidogrel, 0.14 mg/kg prasugrel, 3.57 mg/kg ticlopidine or the same volume of the vehicle and chow diet-fed male mice receiving vehicle (unless otherwise stated, n = 5, 5, 7, 5, and 5, respectively, except n = 6 for the HFD-Ticlopidine group in tolerance tests depicted in panels **g** and **h**). Error bars represent SEM. * $p < 0.05$, ** $p < 0.01$, *** $p < 0.001$, **** $p < 0.0001$ as analyzed by two-way ANOVA with post-hoc Holm-Šídák's test of HFD-Ticlopidine and HFD-Prasugrel vs. HFD-Vehicle groups (**b**) or between all groups (**g**,**h**,**i**), and one-way ANOVA followed by post-hoc Holm-Šídák's test (**d**,**f**). Significant differences vs. respective groups are outlined with color. Scale bar: 100 µm.

Figure 4

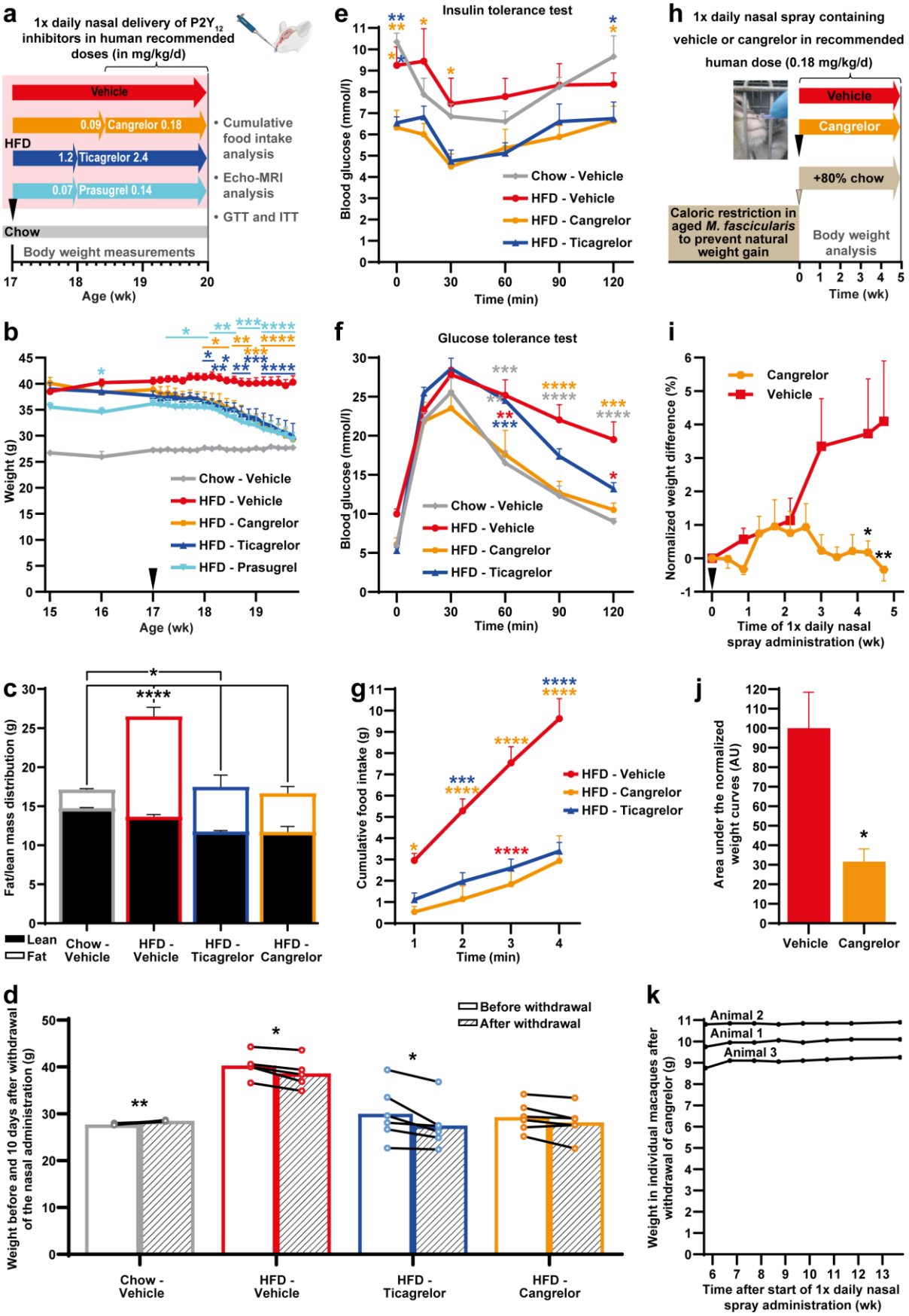

625 **Fig. 4. Anti-obesity effect of nasally administered reversible $P2Y_{12}$ inhibitors in mice and macaques.** (**a-c**) Experimental design to determine the minimal effective dose of the indicated $P2Y_{12}$ inhibitors (**a**), weight (**b**), Echo-MRI-based fat/lean mass distribution analysis (**c**, n = 5),

in chow diet- and HFD-fed male mice nasally administered once a day with vehicle or 0.09 mg/kg followed by switching to 0.18 mg/kg cangrelor from day 10 of the experiment, 1.2 mg/kg followed by switching to 2.4 mg/kg ticagrelor from Week 2, 0.07 mg/kg followed by switching to 0.14 mg/kg prasugrel from Week 2 (unless otherwise stated, n = 5, 5, 6, 6, and 5, respectively). (**d**) Individual weight data in chow diet- and HFD-fed male mice from the above-stated experiment on the last day of nasal administration vehicle, ticagrelor or cangrelor and ten days after withdrawal (n = 5, 5, 6 and 6, respectively). (**e-g**) Insulin (**e**) and glucose (**f**) tolerance tests (n = 5), cumulative food intake (**g**) in chow diet- and HFD-fed male mice from the above-stated experiment nasally administered once a day with vehicle or cangrelor, ticagrelor and prasugrel (unless otherwise stated, n = 5, 5, 5, 6, and 5, respectively). (**h-k**) Experimental design (**h**), normalized weight change (**i**), area under the curve of the normalized weight (**j**) and individual weight data following the drug withdrawal (**k**) in aged male crab-eating macaques (*Macaca fascicularis*) receiving 80% more chow diet compared to normal maintenance conditions in parallel with once-a-day nasal administration of spray containing vehicle or 0.18 mg/kg cangrelor (n = 3). Error bars represent SEM. * $p < 0.05$, ** $p < 0.01$, *** $p < 0.001$, **** $p < 0.0001$ as analyzed by two-way ANOVA with post-hoc Holm-Šídák's test of HFD-Inhibitors vs. HFD-Vehicle groups (**b**) or between all groups (**e-g**,**i**), one-way ANOVA with post-hoc Holm-Šídák's test (**c**), and unpaired two-tailed Student's t-test (**d**,**j**). For the area under the curve analysis, the smallest normalized weight value was used as a baseline. Significant differences vs. respective groups are outlined with color.

Figure 5

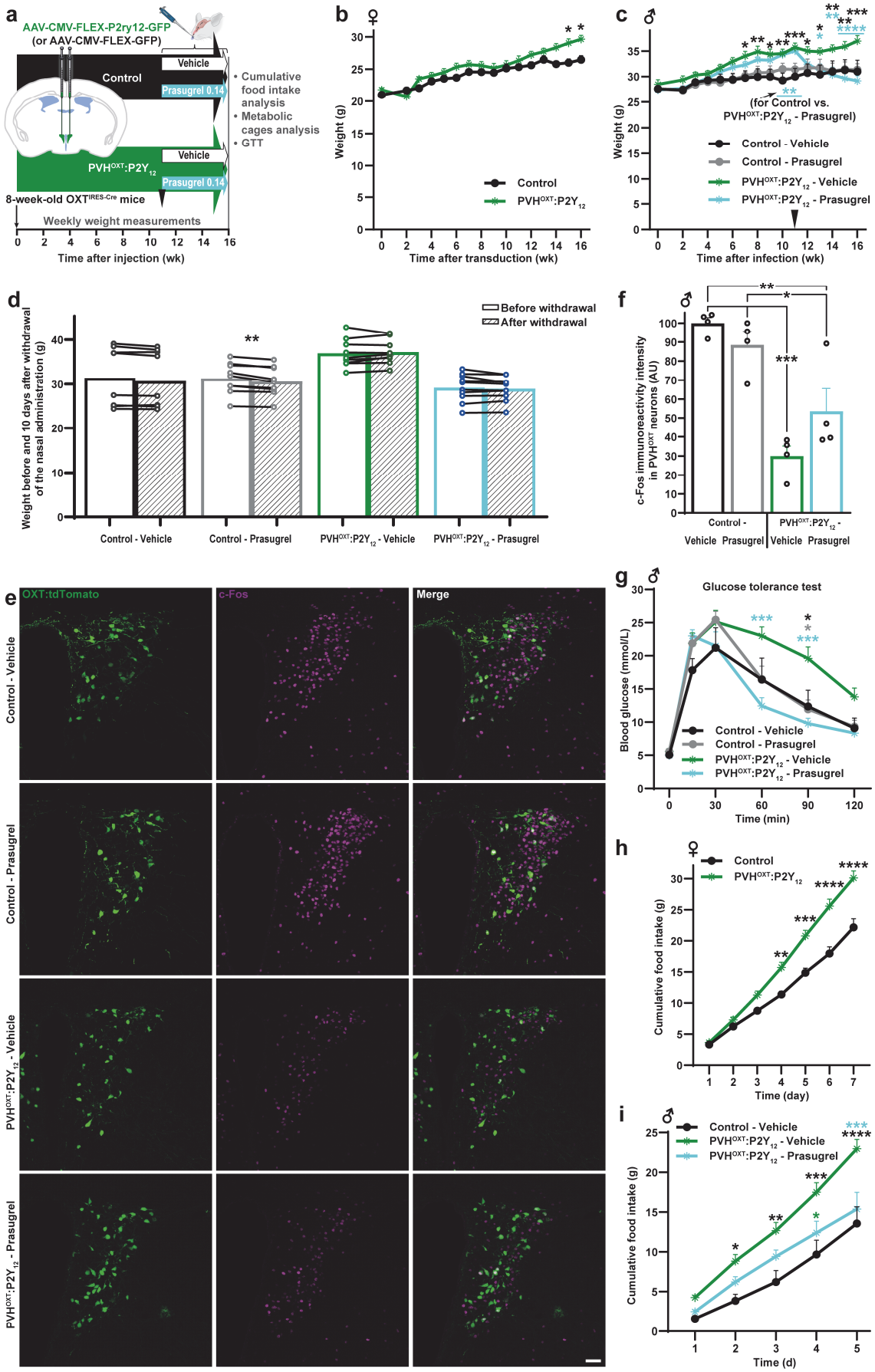
a
AAV-CMV-FLEX-P2ry12-GFP
(or AAV-CMV-FLEX-GFP)
Control
Vehicle
Prasugrel 0.14
PVHOXT:P2Y12
Vehicle
Prasugrel 0.14
• Cumulative food intake analysis
• Metabolic cages analysis
• GTT
8-week-old OXTIRES-Cre mice
Weekly weight measurements
Time after injection (wk)
b
Weight (g)
Control
PVHOXT:P2Y12
Time after transduction (wk)
c
Weight (g)
(for Control vs. PVHOXT:P2Y12 - Prasugrel)
Control - Vehicle
Control - Prasugrel
PVHOXT:P2Y12 - Vehicle
PVHOXT:P2Y12 - Prasugrel
Time after infection (wk)
d
Weight before and 10 days after withdrawal of the nasal administration (g)
Before withdrawal
After withdrawal
Control - Vehicle
Control - Prasugrel
PVHOXT:P2Y12 - Vehicle
PVHOXT:P2Y12 - Prasugrel
f
c-Fos immunoreactivity intensity in PVHOXT neurons (AU)
Control - Vehicle
Control - Prasugrel
PVHOXT:P2Y12 - Vehicle
PVHOXT:P2Y12 - Prasugrel
e
OXT:tdTomato
c-Fos
Merge
Control - Vehicle
Control - Prasugrel
PVHOXT:P2Y12 - Vehicle
PVHOXT:P2Y12 - Prasugrel
g
Glucose tolerance test
Blood glucose (mmol/L)
Control - Vehicle
Control - Prasugrel
PVHOXT:P2Y12 - Vehicle
PVHOXT:P2Y12 - Prasugrel
Time (min)
h
Control
PVHOXT:P2Y12
Cumulative food intake (g)
Time (day)
i
Control - Vehicle
PVHOXT:P2Y12 - Vehicle
PVHOXT:P2Y12 - Prasugrel
Cumulative food intake (g)
Time (d)

Fig. 5. Over-expression of $P2Y_{12}$ in PVH^{OXT} neurons drives hyperphagic obesity and insulin resistance in mice. (**a-c**) Experimental design implementing flip-excision (FLEX) over-expression strategy (**a**), weight (**b**,**c**), individual weight data before and ten days after withdrawal of the drug (**d**), representative microphotographs (**e**) and quantification (**f**) of c-Fos expression in PVH^{OXT} neurons, glucose tolerance test (**g**) and cumulative food intake analyses (**h,i**) in male (**c**,**f,g,i**) and female (**b**,**g**) $OXT^{IRES\text{-}Cre}$ mice after transduction of their PVH with the indicated rAAVs followed by nasal administration of male mice with 0.14 mg/kg/d prasugrel or vehicle. For females n = 7 and 16 for controls and PVH^{OXT}:$P2Y_{12}$, respectively; for males n = 10 for the PVH^{OXT}:$P2Y_{12}$-Prasugrel group and 9 for all others, except c-Fos quantification and food intake analyses depicted in panels **f** and **i**, respectively, where n = 4). Error bars represent SEM. *, $p < 0.05$; **, $p < 0.01$; ***, $p < 0.001$; ****, $p < 0.0001$ as analyzed by two-way ANOVA with Holm-Šídák's test between Control-Vehichle, $P2Y_{12}^{OXT}$OE-Vehicle and $P2Y_{12}^{OXT}$OE-Prasugrel groups (**c**) or between all groups (**b**,**g-i**), one-way ANOVA with Holm-Šídák's test (**f**) and two-tailed paired Student's t-test (**d**). Scale bar: 50 µm.